arXiv:1607.07702v1 [math.NA] 24 Jul 2016

ONLINE INTERPOLATION POINT REFINEMENT FOR REDUCED ORDER MODELS USING A GENETIC ALGORITHM *

SYUZANNA SARGSYAN† STEVEN L. BRUNTON‡ J. NATHAN KUTZ §

Abstract. A genetic algorithm procedure is demonstrated that refines the selection of interpolation points of the discrete empirical interpolation method (DEIM) when used for constructing reduced order models for time dependent and/or parametrized nonlinear partial differential equations (PDEs) with proper orthogonal decomposition. The method achieves nearly optimal interpolation points with only a few generations of the search, making it potentially useful for *online* refinement of the sparse sampling used to construct a projection of the nonlinear terms. With the genetic algorithm, points are optimized to jointly minimize reconstruction error and enable dynamic regime classification. The efficiency of the method is demonstrated on two canonical nonlinear PDEs: the cubic-quintic Ginzburg-Landau equation and the Navier-Stokes equation for flow around a cylinder. Using the former model, the procedure can be compared to the ground-truth optimal interpolation points, showing that the genetic algorithm quickly achieves nearly optimal performance and reduced the reconstruction error by nearly an order of magnitude.

Key words. reduced order modeling, dimensionality reduction, proper orthogonal decomposition, sparse sampling, genetic algorithm, discrete empirical interpolation method

AMS subject classifications. 65L02, 65M02, 37M05, 62H25

1. Introduction. Scientific computation has become critically enabling in almost every field of scientific and engineering study, enabling simulations with modern computers that were thought to be out of reach even a decade ago and suggesting the possibility of exascale computing architectures. The continued scaling of memory, processor speed and parallelization enable studies of increasingly sophisticated multi-scale physical systems. Despite these advances, significant challenges and computational bottlenecks still remain in efficiently computing dynamics of extremely high-dimensional systems, such as high Reynolds turbulent flow. Reduced order models (ROMs) are of growing importance as a critically enabling mathematical framework for reducing the dimension of such large systems. The core of the ROM architecture relies on two key innovations: (i) The POD-Galerkin method [1, 2], which is used for projecting the high-dimensional nonlinear dynamics to a low-dimensional subspace in a principled way, and (ii) sparse sampling (gappy POD) of the state space for interpolating the nonlinear terms required for the subspace projection. The focus of this manuscript is on a sparse sampling innovation for ROMs. Specifically, a method for optimizing sampling locations for both reconstruction and identification of parametrized systems. We propose an algorithm comprised of two components: (i) an *offline* stage that produces initial sparse sensor locations, and (ii) an *online* stage that uses a short, genetic search algorithm for producing nearly optimal sensor locations. The technique optimizes for both reconstruction error and classification efficacy, leading to an attractive *online* modification of commonly used gappy POD methods.

†UNIVERSITY OF WASHINGTON, DEPARTMENT OF APPLIED MATHEMATICS, SEATTLE, WA 98195, USA SSUZIE@UW.EDU

‡UNIVERSITY OF WASHINGTON, DEPARTMENT OF MECHANICAL ENGINEERING, SEATTLE, WA 98195, USA SBRUNTON@UW.EDU

§UNIVERSITY OF WASHINGTON, DEPARTMENT OF APPLIED MATHEMATICS, SEATTLE, WA 98195, USA KUTZ@UW.EDU

*J. N. Kutz acknowledges support from the Air Force Office of Scientific Research (FA9550-15-1-0385).

The importance of sparse sampling of high-dimensional systems, especially those manifesting low-dimensional dynamics, was recognized early on in the ROMs community. Thus sparse sampling has already been established as a critically enabling mathematical framework for model reduction through methods such as gappy POD and its variants [3, 4, 5, 6]. More generally, sparsity promoting methods are of growing importance in physical modeling and scientific computing [7, 8, 9, 10, 11, 12]. The seminal work of Everson and Sirovich [3] first established how the gappy POD could play a transformative role in the mathematical sciences. In their sparse sampling scheme, random measurements were used to perform reconstruction tasks of inner products. Principled selection of the interpolation points, through the gappy POD infrastructure [3, 4, 5, 6] or missing point (best points) estimation (MPE) [13, 14], were quickly incorporated into ROMs to improve performance. More recently, the transformative empirical interpolation method (EIM) [15] and its most successful variant, the POD-tailored discrete empirical interpolation method (DEIM) [16], have provided a greedy, sparse samplimg algorithm that allows for nearly optimal reconstructions of nonlinear terms of the original high-dimensional system. The DEIM approach combines projection with interpolation. Specifically, the DEIM uses selected interpolation indices to specify an interpolation-based projection for a nearly optimal ℓ_2 subspace approximating the nonlinearity.

It is well-known that the various sparse sampling techniques proposed are not optimal, but have been shown to be sufficiently robust to provide accurate reconstructions of the high-dimensional system. The DEIM algorithm has been particularly successful for nonlinear model reduction of time-dependent problems. Interestingly, for parametrized systems, the DEIM algorithm needs to be executed in the various dynamical regimes considered, leading to a library learning mathematical framework [17]. Thus efficient sparse sampling locations for both classification and reconstruction can be computed in an *offline* manner across various dynamical regimes. Again, they are not optimal, but they are robust for building ROMs. We build upon the DEIM library learning framework [17], showing that nearly-optimal sparse sampling can be achieved with a short *online*, genetic algorithm search from the learned DEIM libraries. This improves both the classification and reconstruction accuracy of the sparse sampling, making it an attractive performance enhancer for ROMs.

The paper is outlined as follows: In Sec. 2, the basic ROM architecture is outlined. Section 3 reviews the various innovations of the sparse sampling architecture, including the library building procedure used here. Section 4 develops the genetic search algorithm for *online* improvement of sparse sampling locations. The method advocated here is demonstrated in Sec. 5 on two example problems: the complex cubic-quintic Ginzburg-Landau equation and fluid flow past a circular cylinder. Concluding remarks are provided in Sec. 6.

2. Reduced Order Modeling. In our analysis, we consider a parametrized, high-dimensional system of nonlinear differential equations that arises, for example, from the finite-difference discretization of a partial differential equation. In the formulation proposed, the linear and nonlinear terms for the state vector $\mathbf{u}(t)$ are separated:

$$\frac{d\mathbf{u}(t)}{dt} = L\mathbf{u}(t) + N(\mathbf{u}(t), \mu), \tag{2.1}$$

where $\mathbf{u}(t) = [u_1(t)\ u_2(t)\ \cdots\ u_n(t)]^T \in \mathbb{R}^n$ and $n \gg 1$. Typically, $u_j(t) = u(x_j, t)$ is the value of the field of interest discretized at the spatial location x_j. The linear part

of the dynamics is given by the linear operator $L \in \mathbb{R}^{n\times n}$ and the nonlinear terms are in the vector $N(\mathbf{u}(t)) = [N_1(\mathbf{u}(t),\mu) \quad N_2(\mathbf{u}(t),\mu) \quad \cdots \quad N_n(\mathbf{u}(t),\mu)]^T \in \mathbb{R}^n$. The nonlinear function is evaluated component-wise at the n spatial grid points used for discretization. Note that we have assumed, without loss of generality, that the parametric dependence μ is in the nonlinear term.

Typical discretization schemes for achieving a prescribed spatial resolution and accuracy require the number of discretization points n to be very large, resulting in a high-dimensional state vector. For sufficiently complicated problems where significant spatial refinement is required and/or higher spatial dimension problems (2D or 3D computations, for instance) can potentially lead to a computationally intractable problem where ROMs are necessary. The POD-Galerkin method [1, 2] is a principled dimensionality-reduction scheme that approximates the function $\mathbf{u}(t)$ with rank-r-optimal basis functions where $r \ll n$. These optimal basis functions are computed from a singular value decomposition of a time series of snapshots of the nonlinear dynamical system (2.1). Given the snapshots of the state variable $\mathbf{u}(t_j)$ at $j = 1, 2, \cdots, p$ times, the snapshot matrix $\mathbf{X} = [\mathbf{u}(t_1)\ \mathbf{u}(t_2)\ \cdots\ \mathbf{u}(t_p)] \in \mathbb{R}^{n\times p}$ is constructed and the SVD of $\mathbf{X}$ is computed

$$\mathbf{X} = \mathbf{\Psi}\mathbf{\Sigma}\mathbf{W}^* . \tag{2.2}$$

The r-dimensional basis for optimally approximating $\mathbf{u}(t)$ is given by the first r columns of matrix $\mathbf{\Psi}$, denoted by $\mathbf{\Psi}_r$. The POD-Galerkin approximation is then computed from the following decomposition

$$\mathbf{u}(t) \approx \mathbf{\Psi}_r \mathbf{a}(t) \tag{2.3}$$

where $\mathbf{a}(t) \in \mathbb{R}^r$ is the time-dependent coefficient vector and $r \ll n$. Note that such an expansion implicitly assumes a separation of variables between time and space. Plugging this modal expansion into the governing equation (2.1) and applying orthogonality (multiplying by $\mathbf{\Psi}_r^T$) gives the dimensionally reduced evolution

$$\frac{d\mathbf{a}(t)}{dt} = \mathbf{\Psi}_r^T L \mathbf{\Psi}_r \mathbf{a}(t) + \mathbf{\Psi}_r^T N(\mathbf{\Psi}_r \mathbf{a}(t), \mu) \tag{2.4}$$

where it is noted that $\mathbf{\Psi}_r^T \mathbf{\Psi}_r = \mathbf{I}$, the $r \times r$ identity matrix.

By solving this system of much smaller dimension, the solution of a high-dimensional nonlinear dynamical system can be approximated with optimal (in an ℓ_2 sense) basis functions. Of critical importance is evaluating the nonlinear terms in an efficient way using the gappy POD or DEIM mathematical architecture. Otherwise, the evaluation of the nonlinear terms still requires calculation of functions and inner products with the original dimension n. In certain cases, such as for the quadratic nonlinearity in the Navier-Stokes equations, the nonlinear terms can be computed once in an offline manner. However, parametrized systems generally require repeated evaluation of the nonlinear terms as the POD modes change with μ. Equation (2.4) provides the starting point of the ROM architecture. It also illustrates one of the two critical innovations of ROMs: a principled dimensionality reduction.

3. Gappy Sampling and Discrete Empirical Interpolation Method. In and of itself, the dimensionality reduction provided by the POD method does not ensure that the reduced model (2.4) remains low-dimensional. This is simply due to the evaluation of the nonlinear term $\mathbf{\Psi}_r^T N(\mathbf{\Psi}_r \mathbf{a}(t), \mu)$. Specifically, the nonlinearity forces the evaluation of the nonlinear function and inner products at every time step

when advancing (2.4) with a time-stepping scheme. Such inner products require computations that scale with n, keeping the ROM fixed in the higher dimensional space. In contrast, the linear term $\mathbf{\Psi}_r^T L \mathbf{\Psi}_r$ can be computed once, either at the beginning of the simulation, or in an offline stage. This product of matrices yields a matrix of size $r \times r$, thus requiring computations that scale with r to update the linear portion of the evolution.

To avoid the costly computations associated with approximating $\mathbf{N} = N(\mathbf{\Phi}_r \mathbf{a}(t))$, we compute an approximation to the nonlinearity through projection and interpolation instead of evaluating it directly. A considerable reduction in complexity is achieved by the DEIM, for instance, because evaluating the approximate nonlinear term does not require a prolongation of the reduced state variables back to the original high dimensional state approximation required to evaluate the nonlinearity in the POD approximation. The DEIM therefore improves the efficiency of the POD approximation and achieves a complexity reduction of the nonlinear term with a complexity proportional to the number of reduced variables. The DEIM constructs these specially selected interpolation indices that specify an interpolation-based projection to provide a nearly ℓ_2 optimal subspace approximation to the nonlinear term without the expense of orthogonal projection [16].

3.1. Sparse (Gappy) Sampling. To better understand how the computation of the nonlinearity through projection and interpolation, we consider taking m measurements ($m > r$ with $O(m) \sim O(r)$) of the full state vector $\mathbf{u}$. Specifically, only $m \ll n$ measurements are required for reconstruction, allowing us to define the sparse representation variable $\tilde{\mathbf{u}} \in \mathbb{R}^m$

$$\tilde{\mathbf{u}} = \mathbf{P}\mathbf{u} \tag{3.1}$$

where the measurement matrix $\mathbf{P} \in \mathbb{R}^{m \times n}$ specifies m measurement locations of the full state $\mathbf{u} \in \mathbb{R}^n$. As an example, the measurement matrix might take the form

$$\mathbf{P} = \begin{bmatrix} 1 & 0 & \cdots & & & & & \cdots & 0 \\ 0 & \cdots & 0 & 1 & 0 & \cdots & & \cdots & 0 \\ 0 & \cdots & & & \cdots & 0 & 1 \; 0 & \cdots & 0 \\ \vdots & 0 & & & \cdots & 0 & 0 \; 1 & \cdots & \vdots \\ 0 & \cdots & & & \cdots & 0 & 0 \; 0 & \cdots & 1 \end{bmatrix} \tag{3.2}$$

where measurement locations take on the value of unity and the matrix elements are zero elsewhere. The matrix $\mathbf{P}$ defines a projection onto an m-dimensional measurement space $\tilde{\mathbf{u}}$ that is used to approximate $\mathbf{u}$.

The sparse sampling of (3.1) forms the basis of the *Gappy POD* method introduced by Everson and Sirovich [3]. In their example of eigenface reconstruction, they used a small number of measurements, or gappy data, to reconstruct an entire face. This serves as the basis for approximating the nonlinear inner products in (2.4) and overcoming the computational complexity of the POD reduction. The measurement matrix $\mathbf{P}$ allows for an approximation of the state vector $\mathbf{u}$ from m measurements. The approximation is given by substituting (2.3) into (3.1):

$$\tilde{\mathbf{u}} \approx \mathbf{P} \sum_{j=1}^{m} \tilde{a}_j \psi_j \tag{3.3}$$

where the coefficients $\tilde{a}_j$ minimize the error in approximation

$$\|\tilde{\mathbf{u}} - \mathbf{P}\mathbf{u}\|. \tag{3.4}$$

The goal is to determine the $\tilde{a}_j$ despite the fact that taking inner products of (3.3) can no longer be performed. Specifically, the vector $\tilde{\mathbf{u}}$ is of length m whereas the POD modes are of length n. Implied in this sparse sampling is that the modes $\psi_j(x)$ are in general not orthogonal over the m-dimensional support of $\tilde{\mathbf{u}}$, which is denoted as $s[\tilde{\mathbf{u}}]$. Specifically, the following two relationships hold

$$M_{jk} = (\psi_j, \psi_k) = \delta_{jk} \tag{3.5a}$$

$$M_{jk} = (\psi_j, \psi_k)_{s[\tilde{\mathbf{u}}]} \neq 0 \quad \text{for all } j,k \tag{3.5b}$$

where M_{jk} are the entries of the Hermitian matrix $\mathbf{M}$ and δ_{jk} is the Kroenecker delta function. The fact that the POD modes are not orthogonal on the support $s[\tilde{\mathbf{u}}]$ leads us to consider alternatives for evaluating the vector $\tilde{\mathbf{a}}$.

As demonstrated by Everson and Sirovich [3], the $\tilde{a}_j$ is determined by a least-square fit error algorithm. Specifically, we project the full state vector $\mathbf{u}$ onto the support space and determine the vector $\tilde{\mathbf{a}}$ with the equation:

$$\mathbf{M}\tilde{\mathbf{a}} = \mathbf{f} \tag{3.6}$$

where the elements of the matrix $\mathbf{M}$ are given by (3.5b) and the components of the vector f_k are given by $f_j = (\mathbf{u}, \psi_j)_{s[\tilde{\mathbf{u}}]}$. The pseudo-inverse for determining $\tilde{\mathbf{a}}$ is a least-square fit algorithm. Note that in the event the measurement space is sufficiently dense, or as the support space is the entire space, then $\mathbf{M} = \mathbf{I}$ and $\tilde{\mathbf{a}} \to \mathbf{a}$, thus implying the eigenvalues of $\mathbf{M}$ approach unity as the number of measurements become dense. Once the vector $\tilde{\mathbf{a}}$ is determined, then a reconstruction of the solution can be performed using

$$\mathbf{u}(x,t) \approx \mathbf{\Psi}\tilde{\mathbf{a}}\,. \tag{3.7}$$

It only remains to consider the efficacy of the measurement matrix $\mathbf{P}$. Originally, random measurements were proposed [3]. However, the ROMs community quickly developed principled techniques based upon, for example, minimization of the condition number of $\mathbf{M}$ [4], selection of minima or maxima of POD modes [5], and/or greedy algorithms of EIM/DEIM [15, 16]. Thus m measurement locations were judiciously chosen for the task of accurately interpolating the nonlinear terms in the ROM. This type of sparsity has been commonly used throughout the ROMs community.

3.2. DEIM Algorithm. The DEIM algorithm constructs two low-rank spaces through the SVD: one for the full system using the snapshots matrix $\mathbf{X}$, and a second using the snapshot matrix composed of samples of the nonlinearity alone. Thus a low-rank representation of the nonlinearity is given by

$$\mathbf{N} = [N(\mathbf{u}_1)\ N(\mathbf{u}_2)\ \cdots\ N(\mathbf{u}_p)] = \mathbf{\Xi}\mathbf{\Sigma}_N\mathbf{W}_N^* \tag{3.8}$$

where the matrix $\mathbf{\Xi}$ contains the optimal (in an ℓ_2 sense) basis set for spanning the nonlinearity. Specifically, we consider the rank-m basis set $\mathbf{\Xi}_m = [\boldsymbol{\xi}_1\ \boldsymbol{\xi}_2\ \cdots\ \boldsymbol{\xi}_m]$ that approximates the nonlinear function ($m \ll n$ and $m \sim r$). The approximation to the nonlinearity $\mathbf{N}$ in this SVD basis set is given by:

$$\mathbf{N} \approx \mathbf{\Xi}_m\mathbf{c}(t) \tag{3.9}$$

where $\mathbf{c}(t)$ is similar to $\mathbf{a}(t)$ in (2.3). Since this is a highly overdetermined system, a suitable vector $\mathbf{c}(t)$ can be found by selecting only m rows of the system. The DEIM

TABLE 3.1
DEIM algorithm for finding approximation basis for the nonlinearity and interpolation indices.

DEIM algorithm	
Basis	
• construct snapshot matrix	$\mathbf{X} = [\mathbf{u}(t_1)\ \mathbf{u}(t_2)\ \cdots\ \mathbf{u}(t_p)]$
• construct nonlinear snapshot matrix	$\mathbf{N} = [N(\mathbf{u}(t_1))\ N(\mathbf{u}(t_2))\ \cdots\ N(\mathbf{u}(t_p))]$
• singular value decomposition of $\mathbf{N}$	$\mathbf{N} = \boldsymbol{\Xi}\boldsymbol{\Sigma}_N\mathbf{W}_N^*$
• rank-m approximating basis	$\boldsymbol{\Xi}_m = [\boldsymbol{\xi}_1\ \boldsymbol{\xi}_2\ \cdots\ \boldsymbol{\xi}_m]$
Interpolation Indices (Iteration Loop)	
• choose the first index (initialization)	$[\rho, \gamma_1] = \max\|\boldsymbol{\xi}_1\|$
• approximate $\boldsymbol{\xi}_j$ by $\boldsymbol{\xi}_1, ..., \boldsymbol{\xi}_{j-1}$ at indices $\gamma_1, ..., \gamma_{j-1}$	Solve for $\mathbf{c}$: $\mathbf{P}^T\boldsymbol{\xi}_j = \mathbf{P}^T\boldsymbol{\Xi}_{j-1}\mathbf{c}$ with $\mathbf{P} = [\mathbf{e}_{\gamma_1}\ \cdots\ \mathbf{e}_{\gamma_{j-1}}]$
• select γ_j and loop ($j = 2, 3, ..., m$)	$[\rho, \gamma_j] = \max\|\boldsymbol{\xi}_j - \boldsymbol{\Xi}_{j-1}\mathbf{c}\|$

algorithm provides a greedy search algorithm for selecting an appropriate m rows. Although not guaranteed to be optimal, in practice the row selection tends to provide sampling points that are accurate for reconstruction of the full state.

The DEIM algorithm begins by considering the vectors $\mathbf{e}_{\gamma_j} \in \mathbf{R}^n$ which are the γ_j-th column of the n dimensional identity matrix. We can then construct the projection matrix $\mathbf{P} = [\mathbf{e}_{\gamma_1}\ \mathbf{e}_{\gamma_2}\ \cdots\ \mathbf{e}_{\gamma_m}]$ which is chosen so that $\mathbf{P}^T\boldsymbol{\Xi}_m$ is nonsingular. Then $\mathbf{c}(t)$ is uniquely defined from

$$\mathbf{P}^T\mathbf{N} = \mathbf{P}^T\boldsymbol{\Xi}_m\mathbf{c}(t), \tag{3.10}$$

and thus,

$$\mathbf{N} \approx \boldsymbol{\Xi}_m(\mathbf{P}^T\boldsymbol{\Xi}_m)^{-1}\mathbf{P}^T\mathbf{N}. \tag{3.11}$$

The tremendous advantage of this result for nonlinear model reduction is that the term $\mathbf{P}^T\mathbf{N}$ requires evaluation of nonlinearity only at m indices, where $m \ll n$. The DEIM further proposes a principled method for choosing the basis vectors $\boldsymbol{\xi}_j$ and indices γ_j. The DEIM algorithm, which is based upon a greedy-like search, is detailed in [16] and further demonstrated in Table 3.1.

3.3. Application to Library Learning for parametrized ROMs. The DEIM algorithm is highly effective for determining sampling (sensor) locations. Such sensors can be used with sparse representation and compressive sensing to (i) identify dynamical regimes, (ii) reconstruct the full state of the system, and (iii) provide an efficient nonlinear model reduction and POD-Galerkin prediction for the future state. Given the parametrized nature of the evolution equation (2.4), we use the concept of library building which arises in machine learning from leveraging low-rank "features" from data. In the ROM community, it has recently become an issue of intense investigation. Indeed, a variety of recent works [17, 18, 19, 20, 21, 22, 23, 24, 25, 26] have produced libraries of ROM models that can be selected and/or interpolated through measurement and classification. Before these more formal techniques based upon machine learning were developed, it was already realized that parameter domains could be decomposed into subdomains and a local ROM/POD computed in each subdomain. Patera *et al.* [27] used a partitioning based on a binary tree whereas Amsallem *et al.* [28] used a Voronoi Tessellation of the domain. Such methods were closely related to the work of Du and Gunzburger [29] where the data snapshots were partitioned into

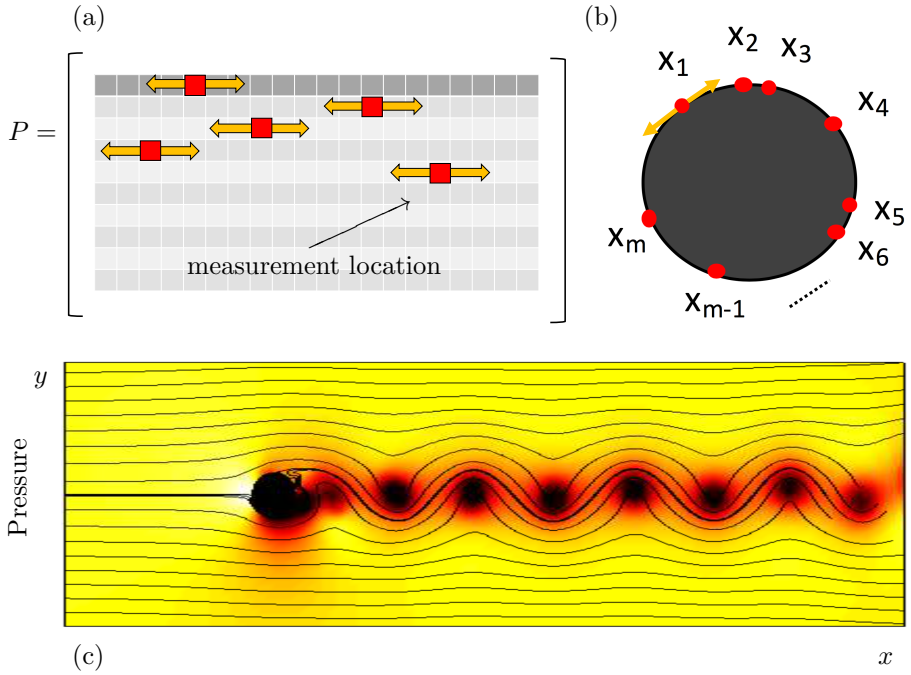

FIG. 4.1. *Illustration of the genetic algorithm search for optimal sparse sampling locations. (a) The measurement matrix P is constructed from the DEIM algorithm across libraries of POD modes [17]. Given that the matrix P has already been demonstrated to produce good interpolation points, the interpolation indices are shifted to nearby locations in a genetic algorithm search for the best interpolation configuration. (b) The algorithm has a practical physical interpretation for the example of flow around a cylinder where the sensor locations are shifted for best performance. (c) The near-optimal interpolation points found from the genetic algorithm are used to both classify the dynamic regime, in this example it discovers the Reynolds number, and to reconstruct the full pressure field (on and off the cylinder) with minimal residual [19].*

subsets and multiple reduced bases computed. Thus the concept of library building is well established and intuitively appealing for parametrized systems.

We capitalize on these recent innovations and build optimal interpolation locations from multiple dynamics states [17]. However, the focus of this work is on computing, in an online fashion, nearly optimal sparse sensor locations from interpolation points found to work across all the libraries in an offline stage. The offline stage uses the DEIM architecture as this method gives good starting points for the interpolation. The genetic algorithm we propose then improves upon the interpolated points by a quick search of nearby interpolation points. It is the pre-computed library structure and interpolation points that allow the genetic algorithm to work with only a short search.

4. Genetic Algorithm for Improved Interpolation. The background Secs. 2 and 3 provide the mathematical framework for the innovations of this paper. Up to this point, the DEIM architecture for parametrized PDEs [17] provides good interpolation points for the ROM method. Our goal is to make the interpolation points optimal or nearly so. Unfortunately, non-convex problems such as this are extremely difficult to optimize, leading to the consideration of genetic algorithms, which are a subset of evolutionary algorithms, for determining near optimal interpolation points.

The genetic algorithm principal is quite simple: given a set of feasible trial solu-

tions (either constrained or unconstrained), an objective (fitness) function is evaluated. The idea is to keep those solutions that give the minimal value of the objective function and mutate them in order to try and do even better. Mutation in our context involves randomly shifting the locations of the interpolation points. Beneficial mutations that give a better minimization, such as good classification and minimal reconstruction error, are kept while those that perform poorly are discarded. The process is repeated through a number of iterations, or *generations*, with the idea that better and better fitness function values are generated via the mutation process.

More precisely, the genetic algorithm can be framed as the constrained optimization problem with the objective function

$$\min \|\tilde{\mathbf{u}} - \mathbf{P}\mathbf{u}\|_2 \quad \text{subject to correct classification} \tag{4.1}$$

where $\mathbf{P}$ is a measurement matrix used for interpolation. Suppose that m mutations, as illustrated in Fig. 4.1, are given for the matrix $\mathbf{P}$ so that

$$j^{\text{th}} \text{ guess is } \mathbf{P}_j\,. \tag{4.2}$$

Thus m solutions are evaluated and compared with each other in order to see which of the solutions generate the smallest objective function since our goal is to minimize it. We can order the guesses so that the first $p < m$ gives the smallest values of $f(\mathbf{P})$. Arranging our data, we then have

$$\begin{aligned} \text{keep} \quad & \mathbf{P}_j \; j = 1, 2, \cdots, p \\ \text{discard} \quad & \mathbf{P}_j \; j = p+1, p+2, \cdots, m\,. \end{aligned} \tag{4.3}$$

Since the first p solutions are the best, these are kept in the next generation. In addition,we now generate $m - p$ new trial solutions that are randomly mutated from the p best solutions. This process is repeated through a finite number of iterations M with the hope that convergence to the optimal, or near-optimal, solution is achieved. Table 4.1 shows the algorithm structure particular to our application. In our simulations, $m = 100$ mutations are produced and $p = 10$ are kept for further mutation. The number of generations is not fixed, but we find that even with $M = 3$, significant improvement in reconstruction error can be achieved.

As we will show, the algorithm provides an efficient and highly effective method for optimizing the interpolation locations, even in a potentially online fashion. A disadvantage of the method is that there are no theorems guaranteeing that the iterations will converge to the optimal solution, and there are many reasons the genetic search can fail. However, we are using it here in a very specific fashion. Specifically, our initial measurement matrix $\mathbf{P}$ is already quite good for classification and reconstruction purposes [17]. Thus the algorithm starts close to the optimal solution. The goal is then to further refine the interpolation points so as to potentially cut down on the reconstruction and classification error. The limited scope of the algorithm mitigates many of the standard pitfalls of the genetic algorithm.

5. Model Problems. Two models help illustrate the principles and success of the genetic search algorithm coupled with DEIM. In the first example, only three interpolation points are necessary for classification and reconstruction [17]. Moreover, for this problem, a brute force search optimization can be performed to rigorously identify the best possible interpolation points. This allows us to compare the method advocated to a ground truth model. In the second example, the classical problem of flow around a cylinder is considered. This model has been ubiquitous in the ROMs community for demonstrating new dimensionality-reduction techniques.

TABLE 4.1
DEIM algorithm for finding approximation basis for the nonlinearity and interpolation indices.

Genetic search algorithm	
• construct initial measurement matrix [17]	$\mathbf{P}$
• perturb measurements and classify	$\mathbf{P} \to \mathbf{P}_1, \mathbf{P}_2, \mathbf{P}_3, \cdots, \mathbf{P}_m$
• keep matrices with correct classification	$\mathbf{P}_k, \mathbf{P}_j, \mathbf{P}_\ell, \cdots$
• save ten best measurement matrices	$\mathbf{P} \to \mathbf{P}_1, \mathbf{P}_2, \cdots, \mathbf{P}_{10}$
• repeat steps for M generations	
• randomly choose one of ten best $\mathbf{P}$ and repeat	

	τ	κ	μ	ν	ϵ	γ	description
β_1	-0.3	-0.05	1.45	0	-0.1	-0.5	3-hump, localized
β_2	-0.3	-0.05	1.4	0	-0.1	-0.5	localized, side lobes
β_3	0.08	0	0.66	-0.1	-0.1	-0.1	breather
β_4	0.125	0	1	-0.6	-0.1	-0.1	exploding soliton
β_5	0.08	-0.05	0.6	-0.1	-0.1	-0.1	fat soliton
β_6	0.08	-0.05	0.5	-0.1	-0.1	-0.1	dissipative soliton

TABLE 5.1
Values of the parameters from equation (5.1) that lead to six distinct dynamical regimes. To exemplify our algorithm, the first, third and fifth regimes will be discussed in this paper.

5.1. Cubic-Quintic Ginzburg-Landau Equation. The Ginzburg-Landau (GL) equation is on of the canonical models of applied mathematics and mathematical physics as it manifests a wide range dynamical behaviors [31]. It is widely used in the study of pattern forming systems, bifurcation theory and dynamical systems. Its appeal stems from its widespread use in the sciences: modeling phenomena as diverse as condensed matter physics to biological waves. The particular variant considered here is the cubic-quintic GL with fourth-order diffusion [32]:

$$iU_t + \left(\frac{1}{2} - i\tau\right) U_{xx} - i\kappa U_{xxxx} + (1 - i\mu)\,|U|^2 U + (\nu - i\epsilon)|U|^4 U - i\gamma U = 0, \quad (5.1)$$

where $U(x,t)$ is a complex valued function of space and time. Under discretization of the spatial variable, $U(x,t)$ becomes a vector $\mathbf{u}$ with n components, i.e. $\mathbf{u}_j(t) = U(x_j,t)$ with $j = 1, 2, \cdots n$.

An efficient and exponentially accurate numerical solution to (5.1) can be found using standard spectral methods [33]. Specifically, the equation is solved by Fourier transforming in the spatial dimension and then time-stepping with an adaptive 4th-order Runge-Kutta method. The extent of the spatial domain is $x \in [-20, 20]$ with $n = 1024$ discretized points. Importantly, in what follows the interpolation indices are dictated by their position away from the center of the computational domain. The center of the domain is at x_0 which is the 513th point in the domain. The interpolation indices demonstrated are relative to this center point.

To generate a variety of dynamical regimes, the parameters of the cubic-quintic GL are tuned to a variety of unique dynamical regimes. The unique parameter regime considered are denoted by the parameter $\beta = (\tau, \kappa, \mu, \nu, \epsilon, \gamma)$ which indicates the specific values chosen. Table 5.1 shows six different parameter regimes that have unique low-dimensional attractors as described in the table. It has been shown in previous work that only three interpolation points are necessary for classification of

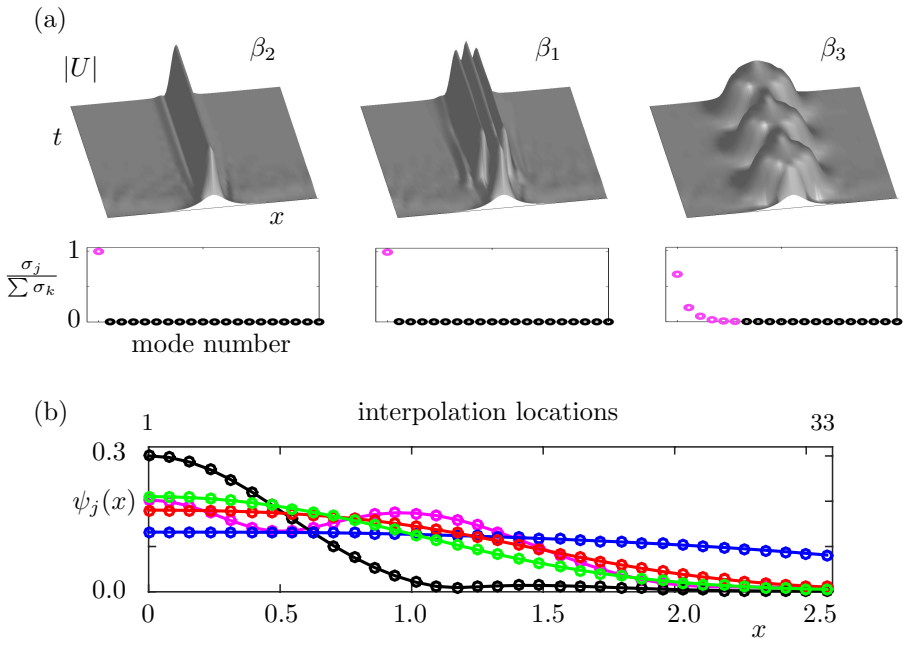

FIG. 5.1. *(a) Evolution dynamics of (5.1) for three different parameter (β) regimes as highlighted in Table 5.1. The intensity evolution is illustrate for $t \in [0, 40]$ on the domain $x \in [-10, 10]$ on a domain discretized with $n = 1024$ points. The subfigure for each evolution denotes the decay of singular values with the magenta dots representing the modes retained in our library Ψ_L. The modes retained account for 99.9% of the total variance. (b) Profile of 5 POD modes $\psi_j(x)$ retained in the library of modes Ψ_L. The figure shows only a small portion of the domain, $x \in [0, 2.6]$, in order to highlight the 33 interpolation points that are possible to use over this selected domain. Note that a majority of the modal structure is contained in this domain, which suggests that this restricted domain may contain optimal interpolation points for the gappy POD evaluation of nonlinear terms for model reduction. Indeed, these 33 interpolation points contain the interpolation points discovered by DEIM as well as the optimal points discovered by exhaustive search (See Figs. 5.2-5.4).*

the dynamical state, state reconstruction and future state prediction [17, 18]. This previous work also explored how to construct the sampling matrix $\mathbf{P}$ from the DEIM algorithm and its multiple dynamical state.

We will execute the genetic algorithm outlined in Table 4.1 for improving the sampling matrix $\mathbf{P}$ initially determined from the algorithm in [17]. Before doing so, we consider a brute force search of the best possible three measurement locations based upon their ability to classify the correct dynamical regime and minimize reconstruction error. Although generally this is an *np*-hard problem, the limited number of sensors and small number of potential locations for sensors allow us to do an exhaustive search for the best interpolation locations. The brute force search first selects all indices triplets (selected from interpolation points 0 to 33 as suggested by [17]) that correctly classify the dynamical regimes in the absence of noisy measurements. From this subset, white noise is added to the measurements and 400 rounds of classification are performed. Only the measurement triplets giving above 95% accuracy for the classification of each dynamical regime are retained. The retained triplets are then sorted by the reconstruction error. Figure 5.2 shows the triplet interpolation points

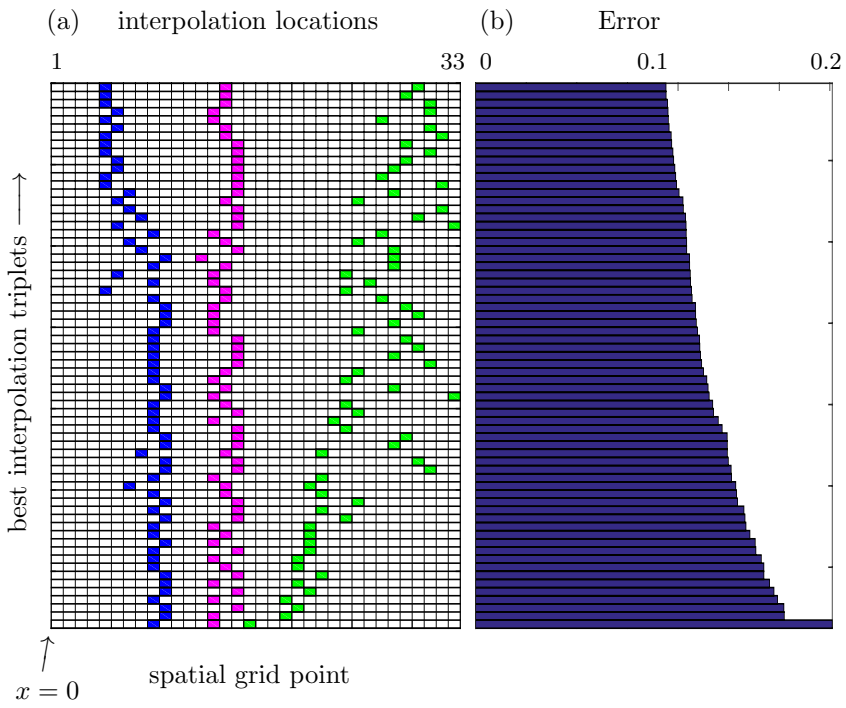

FIG. 5.2. *Results of an exhaustive brute force search for selecting the best three interpolation point triplets that correctly classify the dynamical regimes in the absence of noisy measurements. From this subset, white noise is added to the measurements and 400 rounds of classification are performed. Only the measurement triplets giving above 95% accuracy for the classification of each dynamical regime are retained. The retained triplets are then sorted by the reconstruction error as shown in (a). The corresponding error is shown in (b). Note that the interpolation indices are selected from the first 33 points as shown in Fig. 5.1.*

retained from the exhaustive search with the classification criteria specified and the position of the interpolation points along with the reconstruction error. The DEIM algorithm proposed in [17] produces interpolation points with reconstruction errors nearly an order of magnitude larger than those produced from the exhaustive search. Our objective is to use a genetic algorithm to reduce our error by this order of magnitude and produce interpolation points consistent with some of the best interpolation points displayed in Fig. 5.2.

The brute for search produces a number of interpolation triplets whose reconstruction accuracy are quite similar. Clearly displayed in the graph is the clustering of the interpolation points around critical spatial regions. A histogram of the first (blue), second (magenta) and third (green) interpolation points is shown in Fig. 5.3(a). The first two interpolation points have a narrow distribution around the 4th-8th interpolation points and 12th-16th interpolation points respectively. The third interpolation point is more diffusely spread across a spatial region with improvements demonstrated for interpolation points further to the right in Fig. 5.2(a). This histogram provides critical information about sensor and interpolation point locations. Of note is the fact that the DEIM algorithm always picks the maximum of the first POD mode as an interpolation location. This would correspond to a measurement at $x = 0$. However, none of the candidate triplets retained from a brute force search consider this interpolation point to be important. In fact, the interpolation points starting from the second iteration of the DEIM algorithm are what seem to be important according

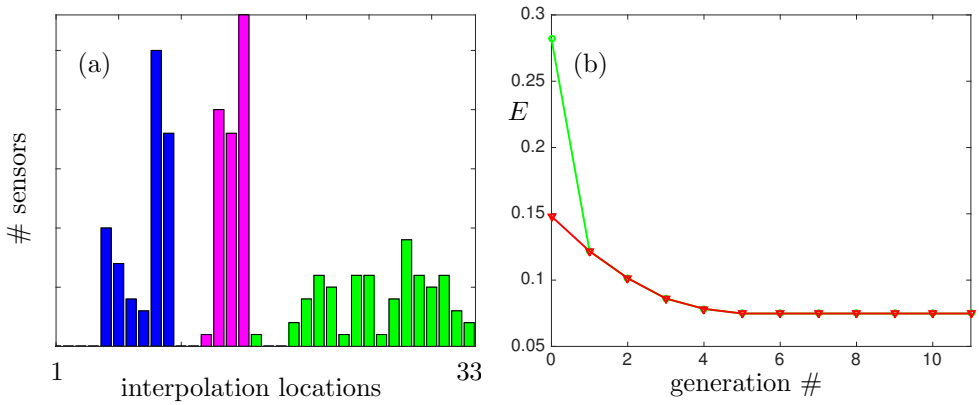

FIG. 5.3. *(a) Histogram of the first (blue), second (magenta) and third (green) interpolation points found from the exhaustive optimization search algorithm in Fig. 5.2. Note that the interpolation indices are selected from the first 33 points as shown in Fig. 5.1. The first two interpolation points are highly localized near key spatial locations. Note that the histograms demonstrate that the first interpolation point selected from the standard DEIM algorithm is not an optimal point. Instead, for this case we can consider the 2nd-4th point instead, shifting the selection of optimal points by one iteration and resulting in the DEIM+1 algorithm, i.e. we generate the first 4 interpolation points from DEIM and drop the first. (b) The genetic algorithm is executed starting form the sparse sampling matrix* $\mathbf{P}$ *of DEIM and DEIM+1 showing that within 2-5 generations nearly optimal interpolation points are found in regards to the error* E*.*

to the brute force search. This leads us to conjecture that we should initially use the triplet pair from the 2nd-4th DEIM points rather than the 1st-3rd DEIM points. We call these the DEIM+1 interpolation points as we shift our measurement indices to the start after the first iteration of DEIM.

The genetic algorithm search can now be enacted from both the DEIM locations computed in [17] and the DEIM+1 locations suggested by the exhaustive search. Figure 5.3(b) shows the convergence of the genetic search optimization procedure starting from both these initial measurement matrices $\mathbf{P}$. It should be noted that the DEIM+1 initially begins with approximately half the error of the standard DEIM algorithm, suggesting it should be used as a default. In this specific scenario, both initial measurement matrices are modified and converge to the near-optimal solution within only 3-5 generations of the search. This is a promising result since the mutations and generations are straightforward to compute and can potentially be done in an online fashion. The benefit from this approach is a reduction of the error by nearly an order of magnitude, making it an attractive scheme.

To finish our analysis, we compare the DEIM architecture against some classic gappy POD and DEIM methods. Figure 5.4 gives an algorithmic comparison of the interpolation point selection of various techniques against the proposed method and the ground truth optimal solution obtained by exhaustive search. Both the reconstruction error and classification accuracy are important in selecting the interpolation indices, and both are represented in panels (b) and (c) of Fig. 5.4. Importantly, the method proposed here, which starts with the DEIM+1 points and does a quick genetic algorithm search produces nearly results that are almost equivalent to the exhaustive search. This is an impressive result given the efficiency of the genetic search and online computation possibilities. And even if one is not interested in executing the genetic search, the DEIM+1 points used for $\mathbf{P}$ provide nearly double the performance

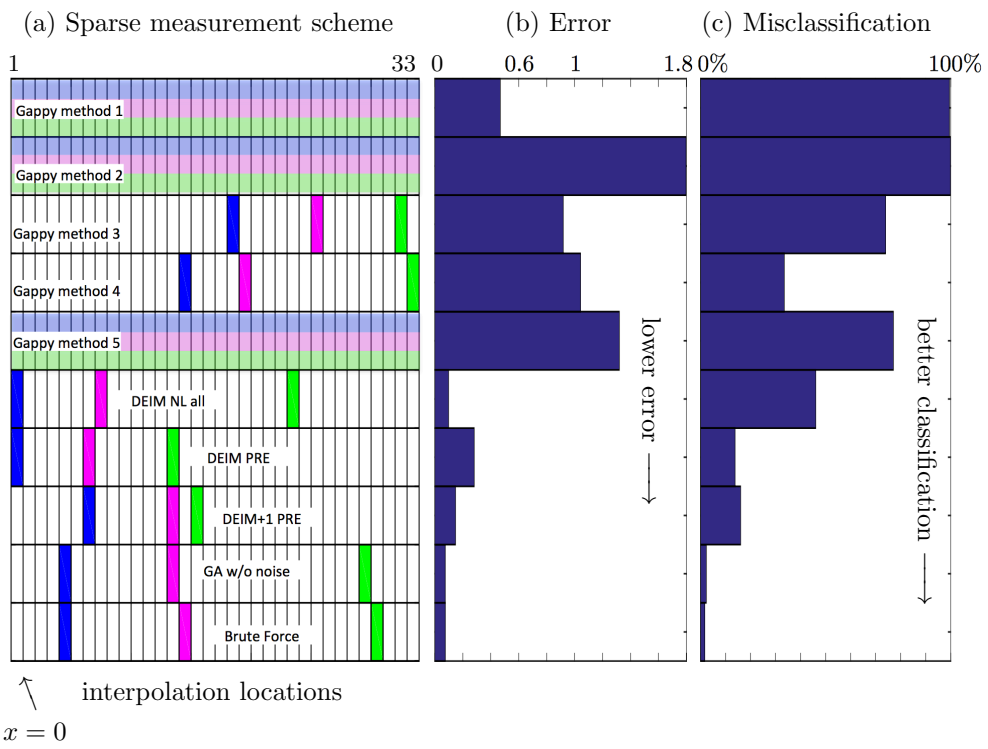

FIG. 5.4. *(a) Comparison of various sparse sampling strategies, including various gappy POD and DEIM methods, against the optimal sparse sampling solution determined by exhaustive search. The first 33 indices of the discretized PDE are shown where the first index corresponds to $x = 0$. The first, second and third measurement locations are denoted by the blue, magenta and green bars respectively. The color bars that span the index locations represents random measurement locations which can be potentially at any of the indices. The accompanying (b) error and (c) misclassification scores are also given. In contrast to many of the other methods, the genetic algorithm proposed produces results that are almost identical to the true optimal solution, making it a viable method for online enhancement of ROMs. The various sparse selection methods are as follows: (i) Gappy method 1: random selection of three indices from interpolation range 1-33 (where the histograms in Figs. 5.1-5.3 suggest the measurements should occur), (ii) Gappy method 2: random selection from all possible interpolation points on the domain, (iii) Gappy method 3: condition number minimization routine for three interpolation points [4], (iv) Gappy method 4: same as Gappy method 3 but with ten interpolation points (i.e. it is now full rank), (v) Gappy method 5: selection of interpolation points from maxima and minima of POD modes [5], (vi) DEIM NL all: DEIM algorithm applied jointly to all the nonlinear terms of all dynamical regimes, (vii) DEIM PRE: algorithm developed in [17], (viii) DEIM+1 PRE: use the algorithm in DEIM PRE but discard the first DEIM point and select from the 2nd-4th DEIM points, (ix) GA: genetic algorithm advocated here, (x) Brute force: optimal solution from exhaustive search*

(in terms of accuracy) versus DEIM.

5.2. Flow Around a Cylinder. The previous example provides an excellent proof-of-concept given that we could compute a ground truth optimal solution. The results suggest that we should start with the DEIM measurement matrix $\mathbf{P}$ and execute the genetic algorithm from there. We apply this method on the classic problem of flow around a cylinder. This problem is also well understood and has already been the subject of studies concerning sparse spatial measurements [19, 34, 35, 36, 37]. Specifically, it is known that for low to moderate Reynolds numbers, the dynamics is spatially low-dimensional and POD approaches have been successful in quantifying the dynamics [34, 38, 39, 40, 41]. The Reynolds number, Re, plays the role of the

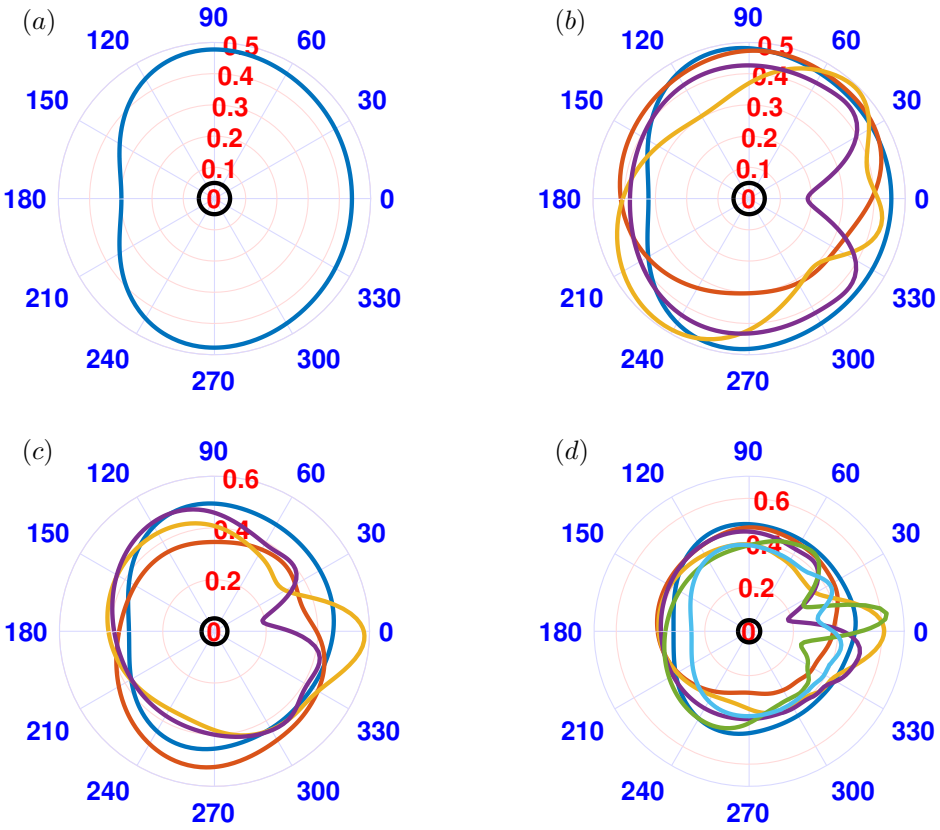

FIG. 5.5. *Dominant POD modes for Reynolds numbers (a) 40, (b) 150, (c) 300 and (d) 1000. The POD modes are plotted in cylindrical coordinates to illustrate the pressure field generated on the cylinder. For low Reynolds numbers (Re = 40), a single dominant POD mode exists. As the Reynolds number increases, more exotic mode structures, which are asymmetric, are manifested. The blue labels are the degrees around the cylinder while the red labels are the amplitudes of the POD pressure modes. The first mode is in blue, followed by red, gold, purple, green and cyan.*

bifurcation parameter μ in (2.1), i.e. it is a parametrized dynamical system.

The data we consider comes from numerical simulations of the incompressible Navier-Stokes equation:

$$\frac{\partial u}{\partial t} + u \cdot \nabla u + \nabla p - \frac{1}{Re}\nabla^2 u = 0 \tag{5.2a}$$

$$\nabla \cdot u = 0 \tag{5.2b}$$

where $u(x, y, t) \in \mathbb{R}^2$ represents the 2D velocity, and $p(x, y, t) \in \mathbb{R}^2$ the corresponding pressure field. The boundary condition are as follows: (i) Constant flow of $u = (1, 0)^T$ at $x = -15$, i.e., the entry of the channel, (ii) Constant pressure of $p = 0$ at $x = 25$, i.e., the end of the channel, and (iii) Neumann boundary conditions, i.e. $\frac{\partial u}{\partial \mathbf{n}} = 0$ on the boundary of the channel and the cylinder (centered at $(x, y) = (0, 0)$ and of radius unity).

We consider the fluid flow for Reynolds number $Re = 40, 150, 300, 1000$ and perform an SVD on the data matrix in order to extract POD modes. The rapid decay of singular values allows us to use a small number of POD modes to describe the fluid

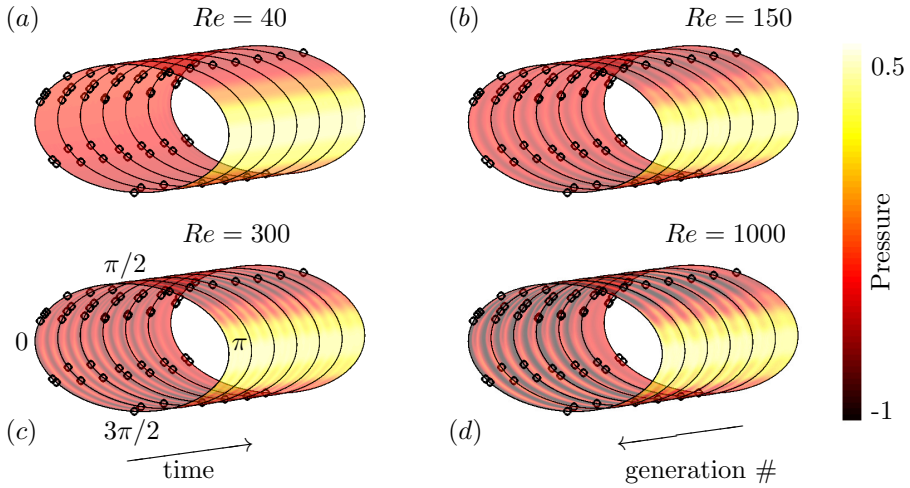

FIG. 5.6. *The heat map on the cylinder shows the dominant, low-dimensional pattern of activity that is used for generating POD modes for Reynolds number (a) 40, (b) 150, (c) 300 and (d) 1000. Overlaid on the heat map are the best sensor/interpolation locations (circles) at each generation of the genetic algorithm scheme for* $m = 10$ *interpolation points over* $M = 7$ *generations of the search. The interpolation locations for each generation in the genetic algorithm start at the back and move forward.*

flow and build local ROMs. The POD modes retained for each Reynolds number is shown in Fig. 5.5. These modes are projected on cylindrical coordinates to better demonstrate the structure of the pressure field generated on the cylinder.

The POD modes can be used to construct a DEIM interpolation matrix $\mathbf{P}$ illustrated in Fig. 4.1. The DEIM interpolation points already provide a good set of interpolation points for classification and reconstruction of the solution. However, the genetic algorithm advocated in this work can be used to adjust the interpolation points and achieve both better classification performance and improved reconstructions. In the cubic-quintic GL equation, the error was improved by nearly an order of magnitude over the standard DEIM approach. For the flow around the cylinder, the error is also improved from the DEIM algorithm, quickly reducing the error with $M = 2$ generations and converging to the nearly optimal interpolation points within $M = 10$ generations. Given the limited number of interpolation points, the genetic search can be computed in an online fashion even for this two-dimensional fluid flow problem.

Figure 5.6 is a composite figure showing the pressure field evolution in time along a the cylinder. The heat map shows the dominant, low-dimensional pattern of activity that is used for generating POD modes. Overlaid on this are the best sensor/interpolation locations at each generation of the genetic algorithm scheme for 10 interpolation points over 7 generations of the search. Note the placement of the interpolation points around the cylinder. Specifically, as the number of generations increases, the interpolation points move to better sampling positions, reducing the error in the ROM. The convergence of the error across 10 generations of the algorithm is shown in Fig. 5.7 along with the final placement of the interpolation points. The near optimal interpolation points are not trivially found. Overall, the DEIM architecture with genetic algorithm search reduces the error by anywhere between a factor of two and an order of magnitude, making it attractive for online error reduction and ROM

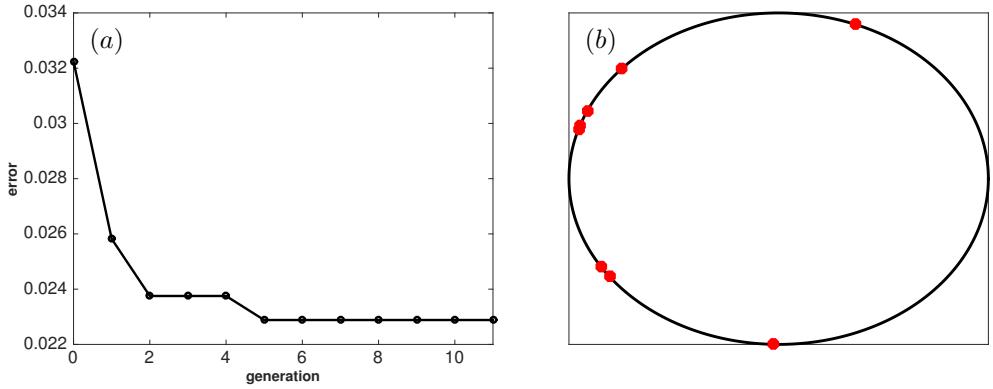

FIG. 5.7. *(a) Error reduction and convergence of the genetic algorithm from an initial DEIM+1 interpolation matrix* $\mathbf{P}$*. Significant error reduction is accomplished in a single generation. A total of* $M = 10$ *generations are shown, illustrating the convergence to the nearly optimal solution. (b) The final position of the interpolation points (red) is shown for 10 interpolation points on the cylinder.*

performance enhancement.

6. Conclusions. ROMs are enabled by two critical steps: (i) the construction of a low-rank subspace where the dynamics can be accurately projected, and (ii) a sparse sampling method that allows for an interpolation-based projection to provide a nearly ℓ_2 optimal subspace approximation to the nonlinear term without the expense of orthogonal projection. Innovations to improve these two aims can improve the outlook of scientific computing methods for modern, high-dimensional simulations that are rapidly approaching exascale levels. These methods also hold promise for real-time control of complex systems, such as turbulence [42]. This work has focused on improving the sparse sampling method commonly used in the literature. In partnership with the DEIM infrastructure, a genetic algorithm was demonstrated to determine nearly optimal sampling locations for producing a subspace approximation of the nonlinear term without the expense of orthogonal projection. The algorithm can be executed in a potentially online manner, improving the error by up to an order-of-magnitude in the examples demonstrated here. In our complex cubic-quintic Ginzburg-Landau equation example, for a fixed number of interpolation points m, the first $m+1$ DEIM interpolation points are computed and the first point is discarded. This DEIM+1 sampling matrix alone can reduce the error by a factor of two before starting the genetic algorithm search.

In general, genetic algorithms are not ideal for optimization since they rarely have guarantees on convergence and have many potential pitfalls. In our case, the DEIM starting point for the interpolation point selection algorithm is already close to the true optimum. Thus the genetic algorithm is not searching blindly in a high-dimensional fitness space. Rather, the algorithm aims to simply make small adjustments and refinements to the sampling matrix in order to maximize the performance of the nonlinear interpolation approximation. In this scenario, many of the commonly observed genetic algorithm failures are of little concern. The method is shown to reduce the error by a substantial amount within only one or two generations, thus making it attractive for implementation in real large-scale simulations where accuracy of the solution may have significant impact on the total computational cost. In comparison to many other sparse sampling strategies used in the literature, it out performs them by

a significant amount both in terms of accuracy and ability to classify the dynamical regime. Indeed, the algorithm refines the sampling matrix $\mathbf{P}$ to be nearly optimal.

Acknowledgements. J. N. Kutz would like to acknowledge support from the Air Force Office of Scientific Research (FA9550-15-1-0385).

REFERENCES

[1] P. J. Holmes, J. L. Lumley, G. Berkooz, and C. W. Rowley. *Turbulence, coherent structures, dynamical systems and symmetry.* Cambridge Monographs in Mechanics. Cambridge University Press, Cambridge, England, 2nd edition, 2012.

[2] P. Benner, S. Gugercin and K. Willcox, *A Survey of Projection-Based Model Reduction Methods for Parametric Dynamical Systems,* SIAM Review , to appear, 2015.

[3] R. Everson and L. Sirovich, "Karhunen-Loéve procedure for gappy data," J. Opt. Soc. Am. A **12**, 1657-1664 (1995).

[4] K. Willcox, *Unsteady flow sensing and estimation via the gappy proper orthogonal decomposition,* Computers and Fluids **35**: 208-226 (2006).

[5] B. Yildirim, C. Chryssostomidis and G.E. Karniadakis, "Efficient sensor placement for ocean measurements using low-dimensional concepts," Ocean Modeling, **273**(3-4), 160-173, (2009).

[6] K. Carlberg, C. Farhat, J. Cortial, and D. Amsallem. *The GNAT method for nonlinear model reduction: Effective implementation and application to computational fluid dynamics and turbulent flows.* Journal of Computational Physics, 242:623–647, 2013.

[7] W. X. Wang, R. Yang, Y. C. Lai, V. Kovanis, and C. Grebogi, "Predicting catastrophes in nonlinear dynamical systems by compressive sensing," *Physical Review Letters*, **106**:154101, (2011).

[8] H. Schaeffer, R. Caflisch, C. D. Hauck, and S. Osher, "Sparse dynamics for partial differential equations," *Proceedings of the National Academy of Sciences*, **110**:6634–6639, (2013).

[9] V. Ozoliņš, R. Lai, R. Caflisch, and S. Osher, "Compressed modes for variational problems in mathematics and physics," *Proceedings of the National Academy of Sciences*, **110**:18368–18373, (2013).

[10] A. Mackey, H. Schaeffer, and S. Osher, "On the compressive spectral method," *Multiscale Modeling & Simulation*, **12**:1800–1827, (2014).

[11] Z. Bai, T. Wimalajeewa, Z. Berger, G. Wang, M. Glauser, and P. K. Varshney, "Low-Dimensional Approach for Reconstruction of Airfoil Data via Compressive Sensing," *AIAA Journal*, **53**(4):920–933, (2014).

[12] S. L. Brunton, J. L. Proctor, and J. N. Kutz, "Discovering governing equations from data by sparse identification of nonlinear dynamical systems," *Proceedings of the National Academy of Sciences*, **113**(15):3932–3937, (2016).

[13] N.C. Nguyen, A. T. Patera, J. Peraire, *A "best points" interpolation method for efficient approximation of parametrized functions.* Int. J. Num. Methods Eng. **73**, 521–543 (2008).

[14] P. Astrid, *Fast reduced order modeling technique for large scale LTV systems,* in Proc. 2004 Am. Control Conf. **1**, 762-767 (2004).

[15] M. Barrault, Y. Maday, N. C. Nguyen, and A. T. Patera, "An 'empirical interpolation' method: Application to efficient reduced-basis discretization of partial differential equations," C. R. Math. Acad. Sci. Paris, 339 (2004), pp. 667-672.

[16] S. Chaturantabut, D. Sorensen, "Nonlinear Model Reduction via Discrete Empirical Interpolation," SIAM J. SCI. COMPUT. **32**, 2737-2764 (2010).

[17] S. Sargsyan, S. L. Brunton and J. N. Kutz, "Nonlinear Model Reduction for Dynamical Systems using Sparse Optimal Sensor Locations from Learned Nonlinear Libraries," Phys. Rev. E **92**, 033304 (2015).

[18] S. L. Brunton, J. H. Tu, I. Bright, J. N. Kutz, "Compressive sensing and low-rank libraries for classification of bifurcation regimes in nonlinear dynamical systems," SIAM J. App. Dyn. Sys., **13**(4): 1716–1732, 2014.

[19] I. Bright, G. Lin, and J. N. Kutz. Compressive sensing and machine learning strategies for characterizing the flow around a cylinder with limited pressure measurements. *Physics of Fluids*, 25:127102–1–127102–15, 2013.

[20] J.L. Proctor, S.L. Brunton, B.W. Brunton and J.N. Kutz "Exploiting sparsity and equation-free architectures in complex systems," European Journal of Physics, **223**: 2665–2684, 2014.

[21] D. Amsallem, R. Tezaur and C. Farhat "Real-time solution of computational problems using

databases of parametric linear reduced-order models with arbitrary underlying meshes," arXiv:1506.07153 (2015).
[22] Y. Choi, D. Amsallem and C. Farhat "Gradient-based Constrained Optimization Using a Database of Linear Reduced-Order Models," arXiv:1506.07849 (2015).
[23] B. Peherstorfer and K. Willcox, "Online Adaptive Model Reduction for Nonlinear Systems via Low-Rank Updates," SIAM Journal on Scientific Computing , to appear, 2015.
[24] B. Peherstorfer and K. Willcox, "Dynamic data-driven reduced-order models," Computer Methods in Applied Mechanics and Engineering," **291**, 21-41 (2015).
[25] B. Peherstorfer and K. Willcox, "Detecting and Adapting to Parameter Changes for Reduced Models of Dynamic Data-driven Application Systems," Procedia Computer Science **51**, 2553-2562, (2015).
[26] E. Kaiser, B. R. Noack, L. Cordier, A. Spohn, M. Segond, M. Abel, G. Daviller, J. Osth, S. Krajnovic and R. K. Niven, "Cluster-based reduced-order modelling of a mixing layer," J. Fluid Mech. **754**, 365–414, (2014).
[27] J. L. Eftang, A. T. Patera, and E. M. Rnquist, "An hp certified reduced-basis method for parameterized elliptic PDEs," Siam SISC, 2010.
[28] D. Amsallem, J. Cortial, and C. Farhat. "On demand CFD-based aeroelastic predictions using a database of reduced-order bases and models," AIAA Conference, 2009.
[29] Q. Du and M. Gunzburger, "Model reduction by proper orthogonal decomposition coupled with centroidal Voronoi tessellation," 2002.
[30] D. Amsallem, M. J. Zahr and K. Washabaugh, "Fast local reduced basis updates for the efficient reduction of nonlinear systems with hyper-reduction," Advances in Computational Mathematics, February 2015, DOI 10.1007/s10444-015-9409-0
[31] M. Cross and P. Hohenberg. Pattern formation out of equilibrium. *Reviews of Modern Physics*, 65:851–1112, 1993.
[32] J. N. Kutz, "Mode-locked soliton lasers," SIAM Rev. **48**:629-678, 2006.
[33] J. N. Kutz. *Data-Driven Modeling & Scientific Computation: Methods for Complex Systems & Big Data*. Oxford University Press, 2013.
[34] D. Venturi and G.E. Karniadakis, "Gappy data and reconstruction procedures for flow past cylinder," J. Fluid Mech., **519**, 315–336 (2004).
[35] K. Kaspers, L. Mathelin, and H. Abou-Kandil, "A statistical learning strategy for flow field estimation from wall-mounted sensors," (submitted), 2015.
[36] K. Kaspers, L. Mathelin, and H. Abou-Kandil, "A machine learning approach for constrained sensor placement," (submitted), 2015.
[37] B. W. Brunton, S. L. Brunton, J. L. Proctor and J. N. Kutz, "Optimal Sensor Placement and Enhanced Sparsity for Classification", (submitted) 2016.
[38] A. E. Deane, I. G. Kevrekidis, G. E. Karniadakis, and S. A. Orszag, "Low-dimensional models for complex geometry flows: Application to grooved channels and circular cylinders," Phys. Fluids, **3**:2337 (1991).
[39] X. Ma and G. E. Karniadakis, "A low-dimensional model for simulating three-dimensional cylinder flow," J. Fluid Mech., **458**:181–190, (2002).
[40] B. Galletti, C. H. Bruneau, and L. Zannetti, "Low-order modelling of laminar flow regimes past a confined square cylinder," J. Fluid Mech., **503**, 161–170 (2004).
[41] E. Liberge and A. Hamdouni, "Reduced order modelling method via proper orthogonal decomposition (POD) for flow around an oscillating cylinder," J. Fluids Struc., **26**, 292–311 (2010).
[42] S. L. Brunton and B. R. Noack, "Closed-loop turbulence control: Progress and challenges," Applied Mechanics Reviews, **67**:050801-1 (2015).